

Better sensing with variable-range interactions

Monika^{1,2}, Leela Ganesh Chandra Lakkaraju², Srijon Ghosh², Aditi Sen(De)²

¹ *Department of Physical Sciences, IISER Berhampur, Berhampur - 760010, India*

² *Harish-Chandra Research Institute, A CI of HBNI, Chhatnag Road, Jhansi, Prayagraj - 211019, India*

The typical bound on parameter estimation, known as the standard quantum limit (SQL), can be surpassed by exploiting quantum resources such as entanglement. To estimate the magnetic probe field, we propose a quantum sensor based on a variable-range many-body quantum spin chain with a moderate transverse magnetic field. We report the threefold benefits of employing a long-range system as a quantum sensor. Firstly, sensors with quasi long-range interactions can always beat SQL for all values of the coordination number while a sensor with long-range interactions does not have this ubiquitous quantum advantage. Secondly, a long-range Hamiltonian outperforms a nearest-neighbor (NN) Hamiltonian in terms of estimating precision. Finally, we observe that the system with long-range interactions can go below SQL in the presence of a high temperature of the initial state while sensors having NN interactions cannot. Furthermore, a sensor based on the long-range Ising Hamiltonian proves to be robust against impurities in the magnetic field and when the time-inhomogeneous dephasing noise acts during interaction of the probe with the system.

I. INTRODUCTION

Gathering information about any physical quantity or parameters involves repeated measurements on the system which inevitably introduces errors in estimation. In a classical domain, the central limit theorem ensures that for repeated measurements on the parameters, the error is proportional to the $\nu^{-1/2}$ known as standard quantum limit (SQL) [1], where ν denotes the total number of measurements performed in the system. However, in a quantum world, it has been realized that the existence of entanglement [2] in the composite system are capable to alter the performance of quantum information processing tasks including quantum communication, computation [3–6]. In a similar spirit, it was discovered that by leveraging quantum resources like entanglement or squeezed states [7, 8], the precision in parameter estimation might further be increased, lowering the error's scaling to the so-called Heisenberg limit (HL) of ν^{-1} [9].

To estimate the strength of the magnetic field interacting with a quantum system, quantum spin systems consisting of N subsystems as probes are routinely employed [10–16] which are then exposed to an external magnetic field for a certain period of time. As a result of the finite energy shifts caused by the magnetic field, the system acquires a relative phase, allowing the corresponding parameters to be estimated by comparing the input and output of the probe after performing measurements [9, 17]. Due to the Cramér-Rao bound [18], the standard deviation in the estimation of the magnetic field for N -body quantum sensors is lower bounded by the inverse of the square root of the Fisher information. Entangled states, in particular, path entangled NOON states [19] and Greenberger-Horne-Zeilinger (GHZ) states [20], help to accomplish in more precise parameter estimation, outperforming the existing precision limitations, $N^{-1/2}$ of utilising uncorrelated probes [21].

Thus, a system governed by a many-body interacting spin Hamiltonian which typically possesses a significant amount of non-local correlations for e.g., entanglement can serve as an efficient probe in quantum metrology [10]. It has also been demonstrated that when the system is fully accessible, preparing the probe's initial state at the critical point, where the correlation length diverges, can be exploited to increase the precision limit [22–26] although such a benefit disappears when the subsystems of the entire system are used. However, such a disadvantage can be remedied by evolving the system periodically [27]. Moreover, recent work shows that the vulnerability of a near-transition of a quantum many-body system from localization to delocalization provides a resource for achieving quantum-enhanced sensitivity in parameter estimation protocol [28]. Towards minimizing the environmental impact on the system, it was suggested [29] that a chain of qubits with only nearest neighbor interaction may be used to construct a quantum sensor in which measurements are made rather than interactions between the sites being modulated. Importantly, quantum advantages obtained in the parameter estimation have been demonstrated in the laboratories using trapped ions [30, 31], thermal vapours of atom [32, 33], nuclear magnetic resonance [34], cold atoms [35], Nitrogen vacancy solid state qubit [36] and in superconducting qubits [37].

It is always fascinating to comprehend how the performance of a quantum sensor is influenced in the presence of noise since setting up and manipulating the isolated system is the ideal situation. Although in the presence of Markovian dephasing noise, quantum sensors can not beat SQL [38, 39], the non-Markovian dynamics of entangled initial states are shown to be better than the unentangled ones, thereby providing quantum advantage [40–45]. To circumvent the detrimental effect of noisy environments on quantum sensors, numerous mechanisms like dynamical decoupling [46–48], error correcting codes [49] are being developed to reach the

Heisenberg limit.

All the aforementioned works have been carried out by using uncorrelated or correlated systems considering only the nearest-neighbor (NN) interactions between subsystems (see Ref. [50] for a recent study on the scaling of quantum Fisher information in long-range interacting systems). However, beyond NN interactions, i.e., long-range interactions naturally arise in physical systems like trapped ions [51, 52], ultracold atoms in optical lattices [53, 54]. Hence quantum sensors built in these platforms should typically involve variable-range interactions which is the main focus of this work. Specifically, the canonical equilibrium state of the XY model with a variable-range interaction in the presence of a magnetic field is employed as the initial state of the quantum sensor. Instead of tuning the interaction between the sites [41], an optimal single-qubit measurement is performed at one of the end points of the spin chain, inducing a flipping mechanism in the entire spin chain during the dynamics of the system (see Appendix A), that results in a GHZ state with high fidelity. To precisely estimate the strength of the probe's magnetic field, the system strongly interacts with the probe for a sufficient amount of time before performing another optimal measurement on a single-qubit for read-out purposes after turning off the magnetic field to be estimated and evolving the system for a suitable time period.

It is important to note that the performance of the sensing protocol is critically dependent on several interrelated system parameters such as the time of initial evolution, measurement setting to create the GHZ state and at the final step for read-out, time in which the probe state interacts with the system, the strength of the magnetic field of the quantum sensor's initial state, and the range of interactions. To begin, we observe that the performance of the quantum sensing protocol used here is most effective when the initial Hamiltonian is the transverse Ising model. We uncover the measurement operators that lead to high fidelity and sensitivity by optimizing over single-qubit rank-1 measurement operators. Furthermore, the time span during which the system should evolve is specified.

The entire examination can provide the platform for addressing the impact of variable range of interactions on the sensitivity. First of all, the range of interactions and coordination number of the initial Hamiltonian are closely connected. We, specifically, report that when the initial state is created involving the quasi-local interactions, quantum sensors can exhibit improved sensitivity by surpassing SQL, and this is true for any coordination number. More significantly, the acquired sensitivity is more than that which can be attained using nearest-neighbor interactions, and this benefit of the quasi long-range Hamiltonian persists even in the presence of a high temperature. However, in case of sensors having long-range interactions, there exists a critical coordination number over which the sensitivity falls below

SQL, exhibiting that the range of interactions can also be deleterious. We also determine that when the magnetic field strength is moderate, the long-range model can outperform the NN model. We demonstrate that the benefit in sensitivity obtained for the quasi-local Hamiltonian persists even in the presence of disorder in the transverse magnetic field and non-Markovian-type dephasing noise.

The paper is organized as follows: Sec. II deals with the quantum sensing protocol adopted here using a variable-range Hamiltonian. In Sec. III, we analyze the performance of a long-range interacting system as a potential candidate for quantum sensors. The beneficial effect of a higher coordination number instead of only the nearest neighbor scenario is also discussed, indicating the effectiveness of using such systems as quantum sensors. The robustness in the estimated uncertainty due to the inevitable presence of impurities in the system is addressed in Sec. IV A while we investigate the effect of local dephasing noise in the estimation protocol in Sec. IV B. Finally, in Sec. V, we summarize the results.

II. STRATEGY OF ESTIMATING PARAMETER IN QUANTUM SPIN MODELS

We present a parameter estimating protocol involving a quantum spin chain, motivated from the recently introduced scheme [29], which is markedly different from the conventional one [10, 13]. Using a variable-range quantum spin chain as the quantum sensor, we systematically demonstrate its enhanced performance in estimating the external probe, i.e., the magnetic field H_{probe} , without controlling the interaction between the qubits and also by performing a local measurement at the initial stage of the protocol and at the time of read-out [29].

Parameter estimation scheme. Precisely, we consider a variable-range interacting Hamiltonian, H , consisting of N spin-1/2 particles, as the quantum sensor for the parameter estimation protocol. The total sensor Hamiltonian consists of two parts

$$H = H_{field} + H_{int}, \quad (1)$$

where H_{field} and H_{int} represent local magnetic field and interaction terms respectively. The exact forms considered in this work will be presented in the later part of the section.

Step 1. Preparation of a suitable state for sensing. The initial state of the sensor is prepared as the canonical equilibrium state of H at inverse temperature $\beta = \frac{1}{k_B \tau}$, with k_B being the Boltzmann constant, and τ being the temperature, i.e., $\rho_{th}(0) = \frac{\exp(-\beta H)}{Z}$, where $Z = \text{Tr}[\exp(-\beta H)]$ represents the partition function of the system. A single qubit arbitrary projective measurement is performed on the first spin of the chain

to initiate the *flipping* mechanism in the entire system. They are written as $P_1(\theta, \phi) = |\mu\rangle\langle\mu|$ and $P_1^\perp(\theta, \phi) = |\mu^\perp\rangle\langle\mu^\perp|$ with $|\mu\rangle = \left(\cos\frac{\theta}{2}|0\rangle + e^{i\phi}\sin\frac{\theta}{2}|1\rangle\right)$, $|\mu^\perp\rangle = \left(\sin\frac{\theta}{2}|0\rangle - e^{i\phi}\cos\frac{\theta}{2}|1\rangle\right)$ such that $0 \leq \theta \leq \pi$ and $0 \leq \phi \leq 2\pi$. By optimizing over θ and ϕ in the measurement, the state obtained after measurement evolves with a global unitary operator, U_{t^*} , governed by the initial Hamiltonian H for a time interval t^* , given by e^{-iHt^*} . Since it is known that $(N-1)$ party GHZ state, $|GHZ\rangle = \frac{1}{\sqrt{2}}(|0\rangle^{\otimes N-1} + |1\rangle^{\otimes N-1})$ possess all the characteristics of being a resource for quantum metrology [7, 55], we maximize the fidelity between the output state obtained after evolution and $(N-1)$ party GHZ state, over the parameters involved in measurements, θ and ϕ . Mathematically, we compute

$$\mathcal{F} = \max_{\theta, \phi} \langle GHZ | \text{Tr}_N(e^{-iHt^*} (P_1(\theta, \phi) \otimes I_{N-1}) \rho_{th}(0) (P_1(\theta, \phi) \otimes I_{N-1}) e^{iHt^*}) | GHZ \rangle \quad (2)$$

where I_{N-1} denotes the identity operator in 2^{N-1} dimension and Tr_N denotes the tracing out of a single site at the edge on which the measurement is not performed, which e.g. can be the site, N .

Step 2. Probe in action. Let us now allow the probe magnetic field to interact with the sensor, by turning off the initial external magnetic field, thereby leading to the evolution of the system under the unitary operator generated by H_{probe} and H_{int} for a time interval t_{int} , i.e., $U_{t_{int}} = e^{-i(H_{probe} + H_{int})t_{int}}$. Hence, the dynamical state at $t = t_{int}$ contains the information about the probe. Again, one switches off the probe Hamiltonian and evolves the system according to e^{-iHt^*} for a fixed time, t^* . Hence, the unitary operators which act on the system for the entire protocol read as

$$U_{total} = U_{t^*} U_{t_{int}} U_{t^*}. \quad (3)$$

Step 3. Read out. Finally, the information about the probe field can be achieved with a high precision by measuring the first qubit using an arbitrary projector, $\{P_1(\theta', \phi'), P_1^\perp(\theta', \phi')\}$. Again, the optimization is performed over the parameters to maximize the estimation of the probe.

A variable-range spin model as a sensor. To illustrate the advantages of constructing a quantum sensor with a long-range quantum spin chain, we consider an XYZ chain with variable-range interactions in the presence of a transverse magnetic field as our workhorse, represented as

$$H_{xyz} = - \sum_{\substack{i < j \\ |i-j| \leq \mathcal{Z}}} \frac{J_{ij}}{4} [J^x \sigma_i^x \sigma_j^x + J^y \sigma_i^y \sigma_j^y + J^z \sigma_i^z \sigma_j^z] + \frac{h^x}{2} \sum_{i=1}^N \sigma_i^x \quad (4)$$

where N is the total number of qubits and σ^k ($k = x, y, z$) are the usual Pauli matrices. Here h^x is the strength of the magnetic field applied along x -direction, representing H_{field} . The first term of H_{xyz} is the interaction Hamiltonian, H_{int} , in which J_{ij} denotes the strength of the interaction between any two sites, i and j which depend on the distance between the sites i and the j and the corresponding power law decay, $J_{ij} \sim A^{-1}|i-j|^{-\alpha}$, with α being the fall-off rate and $A = \sum_{|i-j|=1}^{N-1} |i-j|^{-\alpha}$ being the normalization constant, known as Kac factor [56]. $J_{ij} > 0$ represents the strength of the ferromagnetic interactions between spins and \mathcal{Z} is the coordination number (range of interaction). J^x , J^y , and $J^z \in [0, 1]$ denote the strength of the interaction in the xyz plane. By optimizing them over the said range, we find out that in order to obtain the minimum uncertainty in the parameter estimation scenario, the optimal Hamiltonian in this class is the Ising Hamiltonian, i.e., $J^x = J^y = 0$ and $J^z \neq 0$ (see Fig. 1). Therefore, substituting $J^x = J^y = 0$ and $J^z \neq 0$ in Eq. (4), the sensor Hamiltonian, representing the transverse Ising long-range model, reads as

$$H = - \sum_{\substack{i < j \\ |i-j| \leq \mathcal{Z}}} \frac{J_{ij}}{4} \sigma_i^z \sigma_j^z + \frac{h^x}{2} \sum_{i=1}^N \sigma_i^x. \quad (5)$$

Furthermore, the probe field is taken to be

$$H_{probe} = \frac{\omega}{2} \sum_{i=1}^N \sigma_i^z, \quad (6)$$

where ω is the strength of the magnetic field to be estimated. Additionally, the total magnetization density, along the z -direction, defined as

$$\frac{M^z}{N} \equiv \frac{\langle \sigma^z \rangle}{N} := \frac{1}{2N} \sum_{i=1}^N \sigma_i^z, \quad (7)$$

which is computed to obtain the optimal t^* required for the minimum value of uncertainty (defined below) of the estimated parameter ω .

Let us define how to precisely estimate the frequency parameter ω [1, 38, 57]. For a single qubit, the uncertainty (error) in the estimation can be expressed as

$$\delta\omega = \frac{\sqrt{p(1-p)t_{int}}}{\left| \frac{\partial p}{\partial \omega} \right| \sqrt{T_{total}}}, \quad (8)$$

where $p = \text{Tr}(P_1(\theta', \phi') U_{total} P_1(\theta, \phi) \rho_{th}(0) P_1(\theta, \phi) U_{total}^\dagger)$. Here, T_{total} and t_{int} represent the overall duration of the experiment and the time during which the system evolves under the target magnetic field respectively. By estimating the frequency parameter, we can calculate the amplitude of the target magnetic field. Here, we are assuming t_{int} to be significantly longer than other

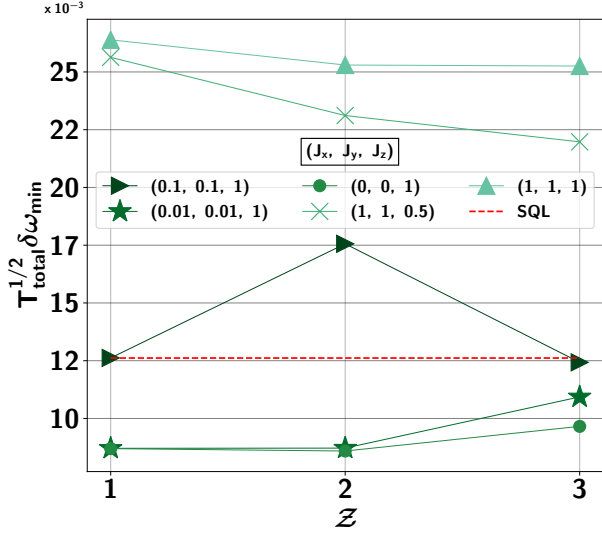


FIG. 1. (Color online) Minimum uncertainty, $\sqrt{T_{total}}\delta\omega_{min}$ (ordinate) vs coordination number Z (abscissa). Different lines correspond to different sets of (J^x, J^y, J^z) . When the values of J^x and J^y are decreasing, along with keeping J^z constant, the value of uncertainty falls below the SQL. This possibly indicates that the long-range Ising model (Eq. 5) is better than the XYZ model as sensors. Both axes are dimensionless.

time scales of the procedure. The main aim in quantum sensing is to minimize the errors in the protocol, thereby maximizing the estimation of parameters, ω . It can be executed by fixing all the other parameters involved in the system including time periods t_{int} as well as t^* , and minimizing $\delta\omega$ which we denote by $\delta\omega_{min}$.

III. BENEFICIAL ROLE OF VARIABLE-RANGE INTERACTION IN QUANTUM METROLOGY

Based on the sensing protocol prescribed in the previous section, we now analyze the performance of a quantum sensor constructed using the long-range transverse Ising model to estimate the uncertainty in determining the strength of the probe magnetic field. For systematic discussion, let us first define some relevant time scales during the protocol apart from the aforementioned evolution time. In the course of finding the minimum uncertainty of the estimated parameter, t_{opt}^* is that particular time for which the evolved state is closest to the GHZ state, thereby providing the maximum advantage in the estimation scenario. To determine this particular time instant while keeping other parameters of the system unchanged, a numerical search has to be performed over a certain range of time, t_{search}^* . Moreover, to indicate the stability of the obtained advantage in uncertainty over time, we define t_{range}^* as the total time duration for which the SQL is surpassed.

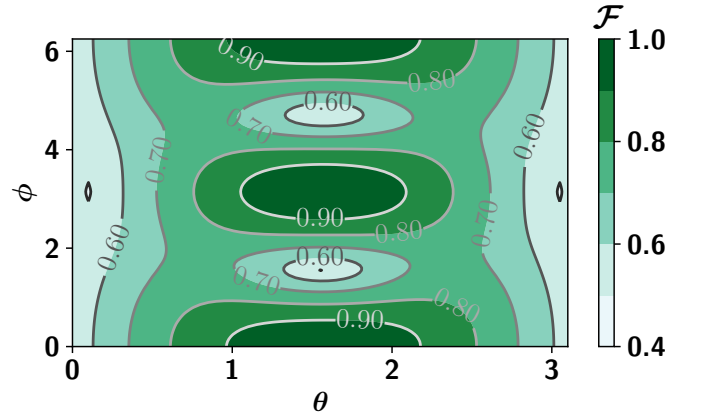


FIG. 2. (Color Online.) Map plot of fidelity (\mathcal{F}) between the resulting and the GHZ state (z-axis) in Eq. (2) with respect to the parameters involved in the measurement operators, θ (x-axis) and ϕ (y-axis) for the nearest-neighbor Hamiltonian. Other parameters in the protocol used here are $h^x = 0.05$, $\beta = 10$, and $\alpha = 1$. Here $N = 4$. All the axes are dimensionless.

Optimal measurement setting

Since the estimation protocol involves arbitrary single qubit projective measurements to initiate the *flipping mechanism* in the system, we optimize over all the θ s and ϕ s to find out the best possible choice of measurement settings to achieve the maximum fidelity, thereby leading to minimum uncertainty. In particular, we observe that the fidelity with the $(N - 1)$ -qubit GHZ state, given in Eq. (2), reaches its maximum value when $\theta = \pi/2$ and $\phi = n\pi$ where $n = 0, 1, 2, \dots$. These specific values of θ and ϕ correspond to the optimal measurement basis, $|\pm\rangle$ where $|\pm\rangle = \frac{|0\rangle \pm |1\rangle}{\sqrt{2}}$ are the eigenvectors of σ^x (see Fig. 2). Further, we perform another arbitrary rank-1 projective measurement on the same qubit on the evolved state, allowing us to extract information from the system by calculating the probability and hence the associated uncertainty in the estimation presented in Eq. (8). We determine that the optimal measurement configuration, in this case, occurs for the basis, $\theta' = \pi/2$ and $\phi' = n\pi/2$ where $n = 1, 3, \dots$, i.e., for the basis, $|\pm i\rangle$ where $|\pm i\rangle = \frac{|0\rangle \pm i|1\rangle}{\sqrt{2}}$, the eigenvectors of σ^y . In the rest of the paper, we calculate $\delta\omega$, by considering these optimal measurement settings. After measurement, we post-select the output and consider the resulting state with +1 eigenvalue only.

Determining the range of t_{search}^*

We are interested to find out t_{search}^* which finally leads to t_{opt}^* , the optimal time upto which the system should evolve according to the unitary U_{t^*} such that \mathcal{F} is maximum. Apart from checking for the optimal \mathcal{F} , the maximal magnetization density also suggests t_{opt}^* since the

optimal measurement on the edge qubit induces flipping (see Appendix A) which implies that the measurement and t_{opt}^* are interrelated. We notice that during the dynamics, there is a specific time at which $\frac{M^z}{N}$ reaches its maximum value for certain system parameters, indicating that all the spins except the spin in which measurement is performed are flipped in the same direction. Moreover, the state of the system at that instant of time shares maximum fidelity with the GHZ state. It turns out that the time at which $\frac{M^z}{N}$ is maximized can indicate the range of t^* from which the optimal time t_{opt}^* can be found for achieving the minimum uncertainty in determining the probe field, as illustrated in Table. I [58, 59].

Precisely, magnetization density exhibits a quasi-periodic nature with respect to time. As time increases, $\frac{M^z}{N}$ initially increases and then reaches its maximum value (see Fig. 3). Furthermore, with the increasing coordination number, the spread of magnetization also increases. Therefore, we fix the value of t_{search}^* as double the value of t_{opt}^* , such that the maximum value of magnetization (i.e., minimum uncertainty) can be unambiguously determined. It is important to notice that as the value of the transverse magnetic field increases, t_{search}^* increases to accommodate spin flipping at larger times. On the other hand, the corresponding $\frac{M^z}{N}$ also decreases. Thus, we observe that it is optimal to consider the value of h^x to be around 0.25, irrespective of the coupling strength and the range of interactions. We will again address the desirable strength of the magnetic field of the sensor in details.

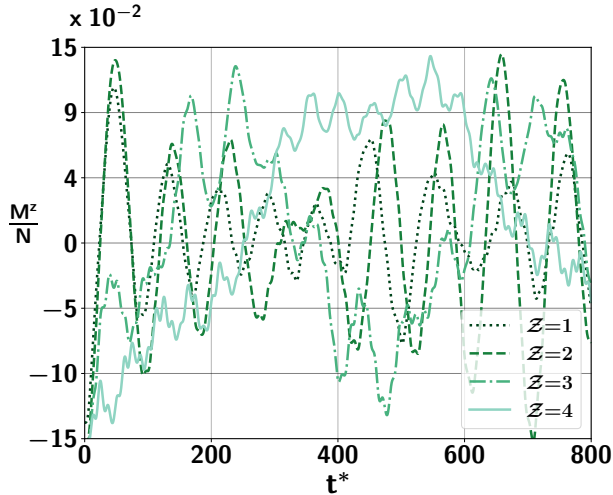


FIG. 3. (Color Online.) Behavior of magnetization density, $\frac{M^z}{N}$ (ordinate) with respect to time duration t^* (abscissa). Different lines represent different values of the coordination number, Z . Here $N = 10$ and $h^x = 0.25$. All other specifications are same as in Fig. 2. Both the axes are dimensionless.

Z	$t_{opt}^*(\frac{M^z}{N})$	$t_{opt}^*(\delta\omega)$
1	46.1	44.7
2	48.3	48.0
3	238.4	239.05
4	546.2	548.25

TABLE I. Optimal times for achieving maximum magnetization density, $t_{opt}^*(\frac{M^z}{N})$ and for minimum uncertainty, $t_{opt}^*(\delta\omega)$ for long-range Ising model with $\alpha = 1$ for different values of Z for $N = 10$.

A. Coordination number vs fall off rate in a quantum sensor

Equipped with the optimal measurement settings and t_{opt}^* , we are now ready to investigate the role of coordination number and the range of interaction on the minimum uncertainty obtained in measuring the magnetic field. Specifically, we now illustrate that both the range of interaction and coordination number is interconnected to estimate ω .

The long-range Ising model possesses different phases characterized by the correlation length between different pairs of spins and parameterized by α , namely, non-local ($0 \leq \alpha \leq 1$), quasi-local ($1 < \alpha < 2$) and local ($\alpha \geq 2$). Note that in physical systems like trapped ions, such Hamiltonian with variable-range interactions following power law naturally appears [60].

Local regime. We report that by preparing the system in the local regime, it is possible to beat SQL for all coordination number Z , as shown in Fig. 5 with $\alpha = 3.0$ although SQL can be surpassed for a limited range of t^* , referred to a t_{range}^* which can be experimentally challenging.

Non-local phase. On the other hand, in the non-local regime, although t_{range}^* increases significantly, indicating the experimental feasibility and the stability of the system, there exists an upper bound on the interaction range, such as $Z = 6$ for $N = 10$ and $\alpha = 1$ (see Fig. 4 (b)), beyond which the system cannot cross the SQL. We find that $\delta\omega$ shows an oscillatory behavior with respect to time of the evolution for various coordination numbers (Z) as depicted in Fig. 4. In other words, when $\alpha \leq 1$, we observe that there exists a critical value of Z up to which the SQL limit is surpassed. For example, strongly coupled model Hamiltonian with coordination numbers, $Z = 7, 8$, and 9 for $N = 10$ cannot beat SQL as depicted in Fig. 5. This illustrates that while increasing the interaction range may enhance the sensitivity, it is not universally effective in building desired quantum sensors. However, from the experimental point of view, we find that the spread of uncertainty oscillations below SQL increases with time, which increases with higher coordination numbers, up to a certain cut-off of Z . This leads to a flexibility in measurements and evolution time.

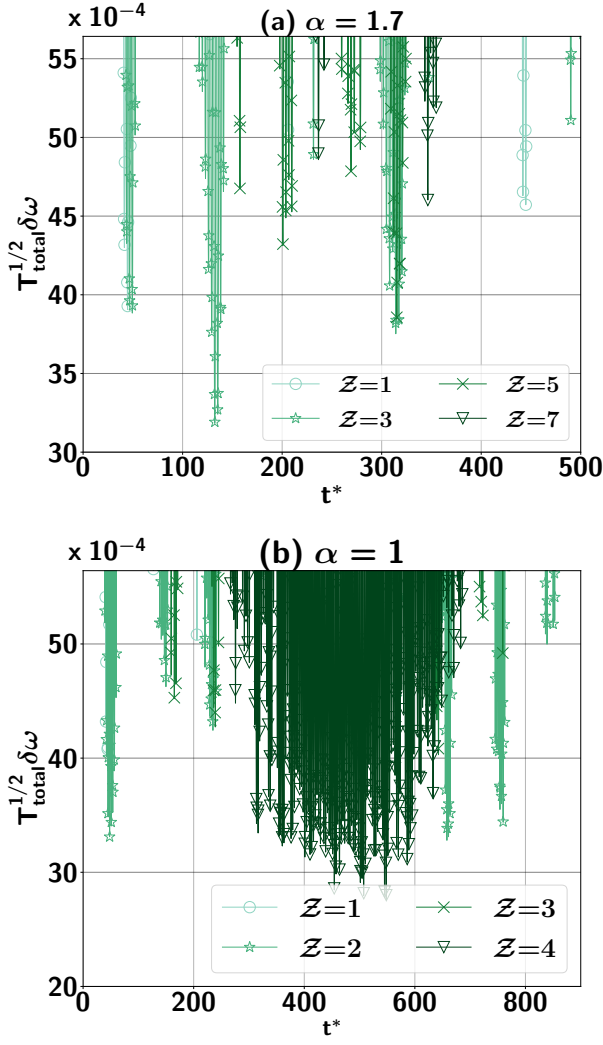


FIG. 4. (Color Online.) $T_{total}^{1/2} \delta \omega$ (ordinate) vs the time interval in which the system evolves initially and in the final step, t^* (abscissa) of the long-range transverse Ising chain as a sensor. Upper and lower panels correspond to two different values of the power law decays, $\alpha = 1.7$ (a) and $\alpha = 1$ (b) respectively. Z is the coordination number of the Ising Hamiltonian. The system size is $N = 10$. The upper limits on the vertical axes represent the standard quantum limit (SQL). Here other parameters involved in the sensing protocols are taken to be $h^x = 0.25$, $t_{int} = 1000\pi$, $\omega = 10^{-6}$, $\alpha = 1$ and $\beta = 10$. Both the axes are dimensionless.

Gain in sensitivity in the quasi-local domain. The interesting trade-off between t^* and the minimum value of $\delta \omega$ emerges when the initial state is prepared in the quasi-local regime having $1 < \alpha < 2$. In particular, in this domain, the sensor can always go below SQL for all values of Z (see Fig. 5 (a)), and the range of t^* is moderately spread, as shown in Fig. 4 for $\alpha = 1.7$. With the decrease of $\alpha \lesssim 1.7$, there exists a critical value of Z above which SQL cannot be exceeded.

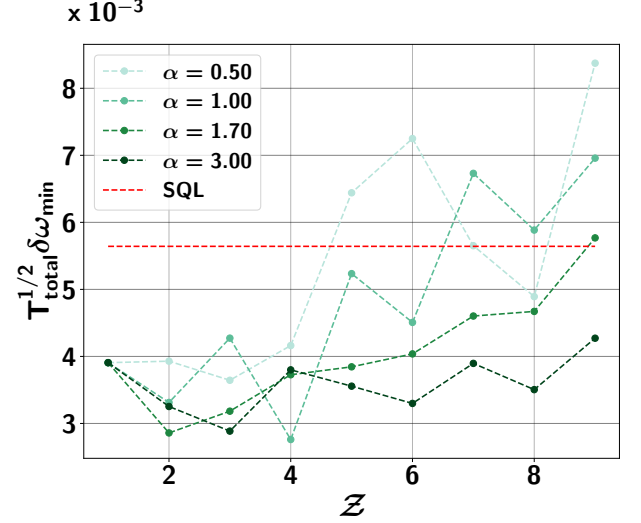


FIG. 5. (Color Online.) **Role of range of interactions on sensors.** $T_{total}^{1/2} \delta \omega_{min}$ against the coordination numbers Z (x-axis) for different fall-off rates (α) of the interaction strength. We notice that the sensor with $\alpha \geq 1.7$ always beats SQL for all values of Z . All other specifications are same as in Fig. 4. Both the axes are dimensionless.

It illustrates that minimum uncertainty can also be used to separate non-local from local regimes of the Ising Hamiltonian. We know that such separation is possible via correlation length. Specifically, if the sensitivity cannot exceed SQL for all Z , we can surely infer that the sensor may involve a long-range Hamiltonian with $\alpha \leq 1$ which no Z simply implies the sensor Hamiltonian to be $\alpha > 2$. The latter observation remains true for the quasi-local Hamiltonian too with $\alpha \lesssim 2$. The entire analysis reveals that quantum sensors built with the long-range Hamiltonian having moderate α and interactions possesses all the desired properties of sensors like low uncertainty and high t_{range}^* , preferable for quantum sensing. With the increase in fall-off rate α , the advantage over SQL becomes more pronounced, and this advantage is sustained over a wider range of interactions. This is due to the fact that, as α increases, the transverse magnetic field eventually reaches a value where it exceeds the next nearest neighbor interaction strength while remaining lower than the nearest neighbor interaction strength [59]. This condition triggers a flipping sequence, resulting in the generation of a polarization wave (see Appendix. A). This flipping sequence allows the system to attain a state after evolution that closely resembles the GHZ state, providing minimum uncertainty in the estimation scenario. We will also show below that to extract its advantage, one also requires to suitably tune the external magnetic field.

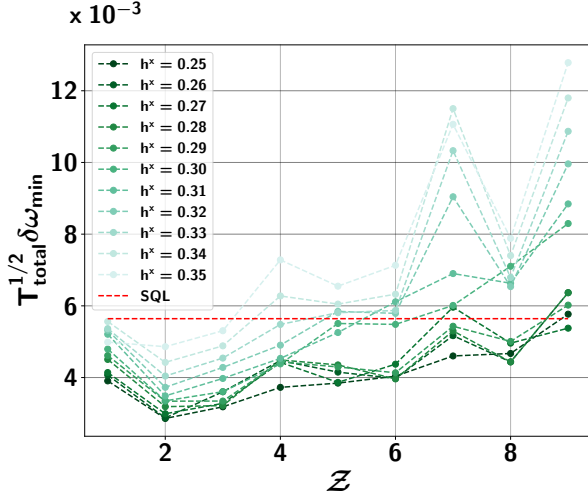


FIG. 6. (Color Online.) Trends of minimum uncertainty $T_{total}^{1/2} \delta \omega_{min}$ (y-axis) with Z (x-axis) for different h^x values. All other specifications except α which is chosen to be 1.7 are same as in Fig. 4. Both the axes are dimensionless.

Effect of external magnetic field

Keeping the system in the quasi-local phase, increasing the value of the magnetic field of the sensor Hamiltonian provides a detrimental effect on the estimated uncertainty of the probe field. It also manifests that for obtaining a quantum advantage in sensors, the interaction between spins is required which, in principle, can create multipartite entanglement. The advantage over SQL becomes less pronounced after reaching a certain value of h^x as demonstrated in Fig. 6. The lowest uncertainty value is consistently observed for $Z = 2$ across all magnetic field strengths. Further, note that after a certain h^x value, the advantage stays only up to $Z = 3$. In addition, the t_{opt}^* value reduces significantly for higher h^x . This behavior is expected because, although for large h^x values, the condition describing the propagation of the stimulated polarization wave is satisfied, the transverse magnetic field becomes too high, leading to the disruption of resonance and resulting in higher uncertainty values.

High temperature can overcome SQL with the aid of long-range interactions

Upto now, the entire analysis is performed with the initial state being prepared at a moderate temperature. However, the presence of thermal noise is an inherent factor that can not be avoided in experimental settings. Therefore, it is crucial to investigate whether the aforementioned advantages persist even when the system interacts with a thermal bath at high temperatures.

Counterintuitively, we find that by incorporating

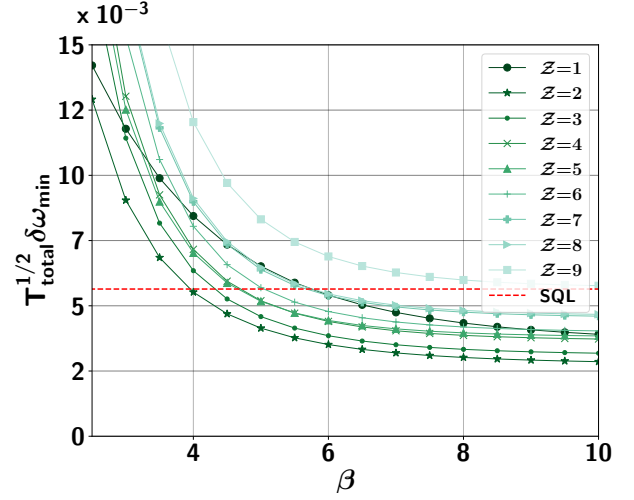


FIG. 7. (Color Online.) Advantage of sensors with long-range Hamiltonian in presence of high temperature. $T_{total}^{1/2} \delta \omega_{min}$ (vertical axis) with β (horizontal axis) for different coordination numbers Z . The red dashed line shows the standard quantum limit (SQL). Here $\alpha = 1.7$. All parameters used here are the same as in Fig. 4. Both the axes are dimensionless.

long-range interactions, it is possible to surpass thermal fluctuations and beat the SQL for higher temperatures where the sensor built with nearest-neighbor interactions fails. We define a critical value of inverse temperature, $\beta_{critical}^Z$, up to which quantum advantage persists for a given range of interaction. We report that

$$\beta_{critical}^{Z=1} > \beta_{critical}^{Z>1} \quad (9)$$

up to certain values of Z for a fixed value of α . In particular, when $1 < \alpha < 2$, there exists values of Z in which $\delta \omega_{min}$ is obtained below SQL for certain low β values which cannot be reached with nearest neighbor model. Specifically, when $\alpha = 1.7$ and $Z = 2$, we find that uncertainty goes below SQL with $\beta \approx 4$ which cannot occur with $Z = 1$ (see Fig. 7). It clearly indicates the advantage of using a long-range Hamiltonian as a quantum sensor in the presence of high temperatures. Notably, as β increases, the minimum uncertainty value exhibits a slight decrement before rapidly reaching a saturation point. Beyond this point, further increments in β do not yield significant improvements in reducing uncertainty. This observation opens up new possibilities for the development of sensors that can outperform SQL, even in the high-temperature limit.

IV. ROBUSTNESS OF SENSORS WITH LONG-RANGE INTERACTIONS AGAINST IMPERFECTIONS

Imperfections can always disturb the performance of the quantum protocols which is also the case for quantum sensors. Here we concentrate on two such situ-

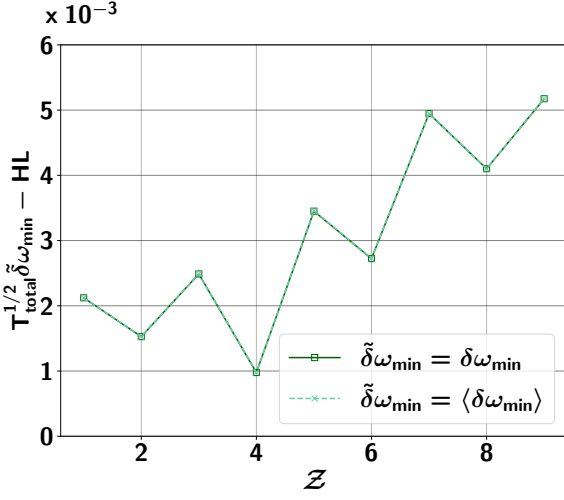


FIG. 8. (Color Online.) **Robustness of sensor against impurities.** Deviation of quenched averaged minimum uncertainty from the Heisenberg limit (HL), i.e., $T^{1/2} \tilde{\omega}_{\min} - \text{HL}$ (ordinate) against Z (abscissa). Let $\langle\delta\omega_{\min}\rangle$ represent the average value of minimum uncertainty in the presence of disorder (dashed cross), and $\delta\omega_{\min}$ represent the same in the absence of disorder (solid square). The Heisenberg limit for system size $N = 10$ is $1/(N\sqrt{t_{\text{int}}})$ with $t_{\text{int}} = 1000\pi$. Mean value \bar{h}_x and standard deviation σ_G are taken to be 0.25 and 0.0001 respectively. Quenched averaging is performed over 500 realizations. All the parameters used here are the same as in Fig. 4. Both the axes are dimensionless.

ations – (1) imperfections enter during the preparation of the initial state which implies the introduction of randomness either in the strength of the magnetic field or in the coupling constants; and (2) when the system is in contact with the bath, the sensing protocols get affected. We will show that the minimum uncertainty is robust against both the defects.

A. Disorder-affected sensors

The amount of uncertainty involved in the parameter estimation protocol through the Cramér-Rao bound [18] clearly states that the error can be minimized by repeating the measurements a large number of times as seen in Eq. (8). Therefore, in the course of repeating the experiment several times, erroneous realization of the probe, measurement device, and most importantly the inherent impurities in the sensor can adversely affect the performance of the sensor. Precisely, the practical implementation of the given protocol is likely to be affected by various sources of noise and disorder, such as environmental perturbations or imperfections in the experimental setup [61–65]. Let us concentrate the effect of impurities present in the system on the performance of the sensor. Here we consider the quenched type of disorder in which the relevant observation time is much

smaller than the equilibration time of the disordered parameter of the system. In order to examine the robustness of the performance of our proposed sensor, we deal with sensor Hamiltonian in which the strength of the magnetic field is chosen randomly from two types of distributions, namely, Gaussian and uniform distribution (see Appendix: B).

Following the same prescription as described in the previous section, we measure the quenched average uncertainty of the estimated parameter, i.e., $\langle\delta\omega_{\min}\rangle$ by averaging over 500 realizations of $\delta\omega$, each of which is obtained individually chosen magnetic field at each site from either a Gaussian or a uniform distribution with a mean value of \bar{h}_x and a certain standard deviation σ_ξ (with $\xi = G, U$) (see Appendix. B), representing the strength of the disorder. We check the convergence of the quenched averaged quantity up to six decimal places.

We observe that the performance of the suggested protocol is not significantly altered by either Gaussian or uniform disorder, in presence of moderate strength of disorder, thus implying the robustness of the proposed model against disorder. In particular, the uncertainty of the estimated parameter ω remains preserved even in the presence of disorder, i.e., it goes below SQL as depicted in Fig. 8 provided the disorder strength is below some critical value, and the strength of magnetic field and other parameters are suitably tuned. These findings demonstrate the potential of our protocol for practical applications in real-world scenarios where the presence of disorder is inevitable.

Furthermore, we find that the maximum standard deviation at which the uncertainty exceeds the SQL value remains almost unaffected by the coordination number. This implies that the largest level of disorder, quantified by the standard deviation above which no advantage over the SQL is obtained, denoted as σ_{\max} , remains relatively constant across all coordination numbers. The value of σ_{\max} exhibits minimal variation regardless of the specific coordination number under consideration which indicates the robustness of the probe against disorder.

B. Environmental effects on parameter estimation

Let us move to a situation when the sensor is in contact with the bath. It was shown that the Ramsey protocol for quantum sensing [38, 66] does not provide the metrological advantage when the Markovian noisy environment is present [38], i.e., the correlation time of the noise is much smaller than the interaction time between the probe and the target field. If the system undergoes evolution under uncorrelated noise so that the corresponding entanglement resource decays rapidly, the separable states and entangled states provide the same uncertainty in estimating a parameter [38]. In a subsequent work [41], it was shown that under a similar

dephasing noise, precise engineering over noise correlation time and characteristic time of the system can achieve better estimation. In that, if the time of dephasing, (T_{dph}), is comparable or larger than the exposure time (t_{int}^{open}) of the target field, the evolution would be non-Markovian-kind and hence quantum advantage can be regained [41]. With the sensor having long-range interactions, we then search for the appropriate interaction time as t_{int}^{open} value that can overcome the SQL.

We perform the evolution in the presence of the environment when the probe is interacting with the target field. The corresponding Lindbladian equation is given as

$$\frac{d}{dt}\rho(t) = -i[H_{int} + H_{probe}, \rho(t)] - \frac{t}{2T_{dph}^2} \sum_{i=1}^N [\sigma_i^z, [\sigma_i^z, \rho(t)]] . \quad (10)$$

Under the zeno-like measurement assumption of $T_{dph} \gg t_{int}^{open}$, the above equation is analytically solvable as

$$\rho(t_{int}^{open}) = \mathcal{M}_1 \left(\mathcal{M}_2 \left(\cdots \mathcal{M}_N \left(\hat{\rho}_I(t_{int}^{open}) \right) \cdots \right) \right), \quad (11)$$

such that $\mathcal{M}_n(\rho) = p'\rho + (1 - p')\sigma_n^z \rho \sigma_n^z$, where $p' = \frac{1 + e^{-(t_{int}^{open}/T_{dph})^2}}{2}$ and $\rho_I(t_{int}^{open}) = e^{-i(H_{int} + H_{probe})t_{int}^{open}} \rho(t^*) e^{i(H_{int} + H_{probe})t_{int}^{open}}$. After the final step of U_{t^*} , we perform the measurement to find the probability. It is important to note that the corresponding $|\partial p / \partial \omega|$ depends on the value of t_{int}^{open} and therefore, the optimization is performed to obtain t_{int}^{open} such that the uncertainty in Eq. (8) is minimized [41, 42, 67]. Notice that the optimization of time span, t_{int} during which the probe interacts with the sensor is not required in the noiseless scenario.

The numerical simulation reveals that the quantum Ising model with long-range interactions outperforms SQL against time-inhomogeneous dephasing noise. The enhanced sensitivity in the case of long-range Hamiltonian is more pronounced than that of the system Hamiltonian with nearest-neighbor interactions (comparing $\delta\omega$ with $\mathcal{Z} = 1$ and $\mathcal{Z} > 1$ as shown in Fig. 9). However, the benefit in sensitivity persists only up to coordination number six when $\alpha = 1$. Furthermore, in the presence of time-inhomogeneous dephasing noise, we note that the improvement over the SQL is smaller compared to the noiseless case (see Figs. 4 and 9).

V. CONCLUSION

Quantum sensors can improve their efficiency in estimating system parameters by utilizing entangled states. The strength of a magnetic field, for example, is estimated by creating interactions between a quantum spin chain and the probe field.

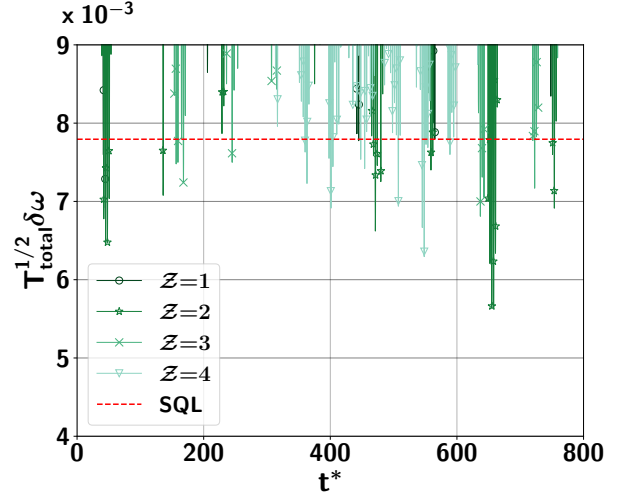


FIG. 9. (Color Online.) **Non-Markovian-type dephasing noise on sensors.** $T_{total}^{1/2}\delta\omega$ (y-axis) with respect to time duration t^* (x-axis) in presence of dephasing noise, described in . Here $h^x = 0.25$, $t_{int}^{open} = 1646$, $T_{dph} = 10^4$, $\beta = 10$, and $\alpha = 1$. All the axes are dimensionless.

We explored the effects of long-range interactions in the spin chain used as a quantum sensor on the estimation of the magnetic field. Specifically, the sensing protocol involves a few critical aspects, including the range of interactions, which divides the spin chain into three distinct phases, non-local, quasi-local, and local, the coordination number, the temperature of the initial state, and the time interval for system evolution and interaction with the probe. The methodology used in this work includes measurements of a single qubit both at the beginning and end.

We found that the quantum sensor based on the transverse Ising chain with long-range interactions does not always exhibit quantum advantage by exceeding the standard quantum limit (SQL) for all coordination numbers, despite the fact that the situation is much better for the quasi-long-range Hamiltonian in terms of precision and time period. Additionally, we discovered that the precision obtained with the inclusion of next-nearest neighbor interactions outperforms the model with nearest-neighbor interactions.

We demonstrated that the quantum advantage may be acquired even when the initial state used for estimating the probe can be prepared in a canonical equilibrium state with moderate to high temperature, provided the system possesses quasi-long range interactions. In the presence of disorder in the transverse magnetic field of the sensor, the quenched average minimum uncertainty remains almost unaltered provided the disorder strength is moderate. We also showed that when the system interacts with non-Markovian-type dephasing noise, the beneficial role of the long-range model still survives.

In summary, our findings emphasize the potential

of long-range interacting quantum systems with decay rates, demonstrating their enhanced metrological performance, robustness against imperfections, and superiority in the presence of environmental interactions. These findings support the fabrication of quantum sensors in physical systems that cannot avoid long-range interactions.

ACKNOWLEDGMENTS

We acknowledge the support from Interdisciplinary Cyber Physical Systems (ICPS) program of the Depart-

ment of Science and Technology (DST), India, Grant No.: DST/ICPS/QuST/Theme- 1/2019/23. We acknowledge the use of [QIClib](#) – a modern C++ library for general purpose quantum information processing and quantum computing (<https://titaschanda.github.io/QIClib>) and cluster computing facility at Harish-Chandra Research Institute. This research was supported in part by the 'INFOSYS scholarship for senior students'.

-
- [1] C. L. Degen, F. Reinhard, and P. Cappellaro, Quantum sensing, *Rev. Mod. Phys.* **89**, 035002 (2017).
 - [2] R. Horodecki, P. Horodecki, M. Horodecki, and K. Horodecki, Quantum entanglement, *Rev. Mod. Phys.* **81**, 865 (2009).
 - [3] A. K. Ekert, Quantum cryptography based on bell's theorem, *Phys. Rev. Lett.* **67**, 661 (1991).
 - [4] C. H. Bennett and S. J. Wiesner, Communication via one- and two-particle operators on einstein-podolsky-rosen states, *Phys. Rev. Lett.* **69**, 2881 (1992).
 - [5] C. H. Bennett, G. Brassard, C. Crépeau, R. Jozsa, A. Peres, and W. K. Wootters, Teleporting an unknown quantum state via dual classical and einstein-podolsky-rosen channels, *Phys. Rev. Lett.* **70**, 1895 (1993).
 - [6] R. Raussendorf and H. J. Briegel, A one-way quantum computer, *Phys. Rev. Lett.* **86**, 5188 (2001).
 - [7] D. J. Wineland, J. J. Bollinger, W. M. Itano, F. L. Moore, and D. J. Heinzen, Spin squeezing and reduced quantum noise in spectroscopy, *Phys. Rev. A* **46**, R6797 (1992).
 - [8] M. Kitagawa and M. Ueda, Squeezed spin states, *Phys. Rev. A* **47**, 5138 (1993).
 - [9] V. Giovannetti, S. Lloyd, and L. Maccone, Quantum metrology, *Phys. Rev. Lett.* **96**, 010401 (2006).
 - [10] P. Zanardi, M. G. A. Paris, and L. Campos Venuti, Quantum criticality as a resource for quantum estimation, *Phys. Rev. A* **78**, 042105 (2008).
 - [11] C. Invernizzi, M. Korbman, L. Campos Venuti, and M. G. A. Paris, Optimal quantum estimation in spin systems at criticality, *Phys. Rev. A* **78**, 042106 (2008).
 - [12] W. L. Boyajian, M. Skotiniotis, W. Dür, and B. Kraus, Compressed quantum metrology for the ising hamiltonian, *Phys. Rev. A* **94**, 062326 (2016).
 - [13] M. Bina, I. Amelio, and M. G. A. Paris, Dicke coupling by feasible local measurements at the superradiant quantum phase transition, *Phys. Rev. E* **93**, 052118 (2016).
 - [14] M. M. Rams, P. Sierant, O. Dutta, P. Horodecki, and J. Zakrzewski, At the limits of criticality-based quantum metrology: Apparent super-heisenberg scaling revisited, *Phys. Rev. X* **8**, 021022 (2018).
 - [15] L. Zhou, J. Kong, Z. Lan, and W. Zhang, Dynamical quantum phase transitions in a spinor bose-einstein condensate and criticality enhanced quantum sensing, *Phys. Rev. Res.* **5**, 013087 (2023).
 - [16] Y. Chu, X. Li, and J. Cai, Strong quantum metrological limit from many-body physics, *Phys. Rev. Lett.* **130**, 170801 (2023).
 - [17] V. Giovannetti, S. Lloyd, and L. Maccone, Advances in quantum metrology, *Nature Photonics* **5**, 222 (2011).
 - [18] H. Cramér, *Mathematical Methods of Statistics*, Goldstone Printed Materials (Princeton University Press, 1946).
 - [19] P. Kok, H. Lee, and J. P. Dowling, Creation of large-photon-number path entanglement conditioned on photodetection, *Phys. Rev. A* **65**, 052104 (2002).
 - [20] D. M. Greenberger, M. A. Horne, and A. Zeilinger, Going Beyond Bell's Theorem, *arXiv e-prints*, [arXiv:0712.0921](#) (2007), [arXiv:0712.0921 \[quant-ph\]](#).
 - [21] C. M. Caves, Quantum-mechanical noise in an interferometer, *Phys. Rev. D* **23**, 1693 (1981).
 - [22] P. Zanardi and N. Paunković, Ground state overlap and quantum phase transitions, *Phys. Rev. E* **74**, 031123 (2006).
 - [23] P. Zanardi, H. T. Quan, X. Wang, and C. P. Sun, Mixed-state fidelity and quantum criticality at finite temperature, *Phys. Rev. A* **75**, 032109 (2007).
 - [24] P. Zanardi, M. G. A. Paris, and L. Campos Venuti, Quantum criticality as a resource for quantum estimation, *Phys. Rev. A* **78**, 042105 (2008).
 - [25] C. Invernizzi, M. Korbman, L. Campos Venuti, and M. G. A. Paris, Optimal quantum estimation in spin systems at criticality, *Phys. Rev. A* **78**, 042106 (2008).
 - [26] M. M. Rams, P. Sierant, O. Dutta, P. Horodecki, and J. Zakrzewski, At the limits of criticality-based quantum metrology: Apparent super-heisenberg scaling revisited, *Phys. Rev. X* **8**, 021022 (2018).
 - [27] U. Mishra and A. Bayat, Driving enhanced quantum sensing in partially accessible many-body systems, *Phys. Rev. Lett.* **127**, 080504 (2021).
 - [28] A. Sahoo, U. Mishra, and D. Rakshit, Localization driven quantum sensing (2023), [arXiv:2305.02315 \[quant-ph\]](#).
 - [29] A. Yoshinaga, M. Tatsuoka, and Y. Matsuzaki, Entanglement-enhanced sensing using a chain of qubits with always-on nearest-neighbor interactions, *Phys. Rev. A* **103**, 062602 (2021).
 - [30] R. Maiwald, D. Leibfried, J. Britton, J. C. Bergquist, G. Leuchs, and D. J. Wineland, Stylus ion trap for enhanced access and sensing, *Nature Physics* **5**, 551 (2009).
 - [31] F. Wolf and P. O. Schmidt, Quantum sensing of oscillating electric fields with trapped ions, *Measurement: Sensors* **18**, 100271 (2021).
 - [32] J. Kitching, S. Knappe, and E. A. Donley, Atomic sensors–

- a review, *IEEE Sensors Journal* **11**, 1749 (2011).
- [33] D. Budker and M. Romalis, Optical magnetometry, *Nature physics* **3**, 227 (2007).
 - [34] T. Staudacher, F. Shi, S. Pezzagna, J. Meijer, J. Du, C. A. Meriles, F. Reinhard, and J. Wrachtrup, Nuclear magnetic resonance spectroscopy on a (5-nanometer)³ sample volume, *Science* **339**, 561 (2013).
 - [35] J. Huang, S. Wu, H. Zhong, and C. Lee, *Annual Review of Cold Atoms and Molecules*, 365 (2014).
 - [36] S. Kolkowitz, A. Safira, A. High, R. Devlin, S. Choi, Q. Unterreithmeier, D. Patterson, A. Zibrov, V. Manucharyan, H. Park, *et al.*, Probing johnson noise and ballistic transport in normal metals with a single-spin qubit, *Science* **347**, 1129 (2015).
 - [37] F. Yan, J. Bylander, S. Gustavsson, F. Yoshihara, K. Harrabi, D. G. Cory, T. P. Orlando, Y. Nakamura, J.-S. Tsai, and W. D. Oliver, Spectroscopy of low-frequency noise and its temperature dependence in a superconducting qubit, *Phys. Rev. B* **85**, 174521 (2012).
 - [38] S. F. Huelga, C. Macchiavello, T. Pellizzari, A. K. Ekert, M. B. Plenio, and J. I. Cirac, Improvement of frequency standards with quantum entanglement, *Phys. Rev. Lett.* **79**, 3865 (1997).
 - [39] J. F. Haase, A. Smirne, S. Huelga, J. Kołodynski, and R. Demkowicz-Dobrzanski, Precision limits in quantum metrology with open quantum systems, *Quantum Measurements and Quantum Metrology* **5**, 13 (2016).
 - [40] J. A. Jones, S. D. Karlen, J. Fitzsimons, A. Ardavan, S. C. Benjamin, G. A. D. Briggs, and J. J. Morton, Magnetic field sensing beyond the standard quantum limit using 10-spin noon states, *science* **324**, 1166 (2009).
 - [41] Y. Matsuzaki, S. C. Benjamin, and J. Fitzsimons, Magnetic field sensing beyond the standard quantum limit under the effect of decoherence, *Phys. Rev. A* **84**, 012103 (2011).
 - [42] A. W. Chin, S. F. Huelga, and M. B. Plenio, Quantum metrology in non-markovian environments, *Phys. Rev. Lett.* **109**, 233601 (2012).
 - [43] K. Macieszczak, Zeno limit in frequency estimation with non-markovian environments, *Phys. Rev. A* **92**, 010102 (2015).
 - [44] A. Bhattacharyya, A. Ghoshal, and U. Sen, Restoring metrological quantum advantage of measurement precision in noisy scenario (2022), [arXiv:2211.05537 \[quant-ph\]](https://arxiv.org/abs/2211.05537).
 - [45] A. Bhattacharyya, A. Ghoshal, and U. Sen, Disorder-induced enhancement of precision in quantum metrology (2023), [arXiv:2212.08523 \[quant-ph\]](https://arxiv.org/abs/2212.08523).
 - [46] L. Viola, E. Knill, and S. Lloyd, Dynamical decoupling of open quantum systems, *Phys. Rev. Lett.* **82**, 2417 (1999).
 - [47] L. M. Pham, N. Bar-Gill, C. Belthangady, D. Le Sage, P. Cappellaro, M. D. Lukin, A. Yacoby, and R. L. Walsworth, Enhanced solid-state multispin metrology using dynamical decoupling, *Phys. Rev. B* **86**, 045214 (2012).
 - [48] Z. Yang and H. Zhang, Evolution of surface states of antiferromagnetic topological insulator mnbizte4 with tuning the surface magnetization, *New Journal of Physics* **24**, 073034 (2022).
 - [49] E. M. Kessler, I. Lovchinsky, A. O. Sushkov, and M. D. Lukin, Quantum error correction for metrology, *Phys. Rev. Lett.* **112**, 150802 (2014).
 - [50] R. Yousefjani, X. He, and A. Bayat, Long-range interacting stark many-body probes with super-heisenberg precision (2023), [arXiv:2307.03904 \[quant-ph\]](https://arxiv.org/abs/2307.03904).
 - [51] L. Lamata, J. León, T. Schätz, and E. Solano, Dirac equation and quantum relativistic effects in a single trapped ion, *Phys. Rev. Lett.* **98**, 253005 (2007).
 - [52] R. Gerritsma, G. Kirchmair, F. Zähringer, E. Solano, R. Blatt, and C. Roos, Quantum simulation of the dirac equation, *Nature* **463**, 68 (2010).
 - [53] M. Cramer, A. Bernard, N. Fabbri, L. Fallani, C. Fort, S. Rosi, F. Caruso, M. Inguscio, and M. B. Plenio, Spatial entanglement of bosons in optical lattices, *Nature communications* **4**, 2161 (2013).
 - [54] O. Mandel, M. Greiner, A. Widera, T. Rom, T. W. Hänsch, and I. Bloch, Controlled collisions for multi-particle entanglement of optically trapped atoms, *Nature* **425**, 937 (2003).
 - [55] N. D. Mermin, Extreme quantum entanglement in a superposition of macroscopically distinct states, *Phys. Rev. Lett.* **65**, 1838 (1990).
 - [56] M. Kac, G. Uhlenbeck, and P. Hemmer, On the van der waals theory of the vapor-liquid equilibrium. i. discussion of a one-dimensional model, *Journal of Mathematical Physics* **4**, 216 (1963).
 - [57] Y. Takeuchi, Y. Matsuzaki, K. Miyanishi, T. Sugiyama, and W. J. Munro, Quantum remote sensing with asymmetric information gain, *Phys. Rev. A* **99**, 022325 (2019).
 - [58] J.-S. Lee and A. K. Khitrin, Stimulated wave of polarization in a one-dimensional ising chain, *Phys. Rev. A* **71**, 062338 (2005).
 - [59] G. B. Furman, S. D. Goren, J.-S. Lee, A. K. Khitrin, V. M. Meerovich, and V. L. Sokolovsky, Stimulated wave of polarization in spin chains, *Phys. Rev. B* **74**, 054404 (2006).
 - [60] D. Vodola, L. Lepori, E. Ercolessi, and G. Pupillo, Long-range ising and kitaev models: phases, correlations and edge modes, *New Journal of Physics* **18**, 015001 (2015).
 - [61] C. Fort, L. Fallani, V. Guarrera, J. E. Lye, M. Modugno, D. S. Wiersma, and M. Inguscio, Effect of optical disorder and single defects on the expansion of a bose-einstein condensate in a one-dimensional waveguide, *Phys. Rev. Lett.* **95**, 170410 (2005).
 - [62] L. Fallani, J. E. Lye, V. Guarrera, C. Fort, and M. Inguscio, Ultracold atoms in a disordered crystal of light: Towards a bose glass, *Phys. Rev. Lett.* **98**, 130404 (2007).
 - [63] M. White, M. Pasienski, D. McKay, S. Q. Zhou, D. Ceperley, and B. DeMarco, Strongly interacting bosons in a disordered optical lattice, *Phys. Rev. Lett.* **102**, 055301 (2009).
 - [64] B. Shapiro, Cold atoms in the presence of disorder, *Journal of Physics A: Mathematical and Theoretical* **45**, 143001 (2012).
 - [65] V. Ahufinger, L. Sanchez-Palencia, A. Kantian, A. Sanpera, and M. Lewenstein, Disordered ultracold atomic gases in optical lattices: A case study of fermi-bose mixtures, *Phys. Rev. A* **72**, 063616 (2005).
 - [66] H. Lee, P. Kok, and J. P. Dowling, A quantum rosetta stone for interferometry, *Journal of Modern Optics* **49**, 2325 (2002), <https://doi.org/10.1080/0950034021000011536>.
 - [67] M. Tatsuta, Y. Matsuzaki, and A. Shimizu, Quantum metrology with generalized cat states, *Phys. Rev. A* **100**, 032318 (2019).
 - [68] A. Kauch, P. Worm, P. Prauhart, M. Innerberger, C. Watzenböck, and K. Held, Enhancement of impact ionization in hubbard clusters by disorder and next-nearest-neighbor hopping, *Phys. Rev. B* **102**, 245125 (2020).
 - [69] H. Gimperlein, S. Wessel, J. Schmiedmayer, and L. San-

tos, Ultracold atoms in optical lattices with random on-site interactions, *Phys. Rev. Lett.* **95**, 170401 (2005).

- [70] P. Sierant, D. Delande, and J. Zakrzewski, Many-body localization due to random interactions, *Phys. Rev. A* **95**, 021601 (2017).

Appendix A: Secular Hamiltonian for long-range interacting systems: Condition for the generation of spin-polarization wave

The spin polarization wave can be generated using the Ising model with long-range interactions. In the work by Furman *et al.* [59], it was shown that given an initial state, $|100 \dots 0\rangle$ where $|0\rangle$ and $|1\rangle$ are ground and first excited states of the σ^z Hamiltonian, the evolution governed by the long-range Hamiltonian (in Eq. (5)) can induce a spin polarization wave. To obtain the effective (secular) Hamiltonian responsible for the generation of this spin polarization wave, the Hamiltonian is transformed into the interaction picture, and the time-dependent part in the interaction picture is neglected. In this context, all the spins are irradiated at resonant frequencies by perturbation term $H_{field} = h^x \sum_i \sigma_i^x$. In their study, they have proven that by considering the limit $J_{ij} \gg h^x$ for $\alpha = 3$, the secular Hamiltonian can be expressed as follows:

$$H_{eff} = \frac{h^x}{2} \sum_{i=\mathcal{Z}+1}^{N-\mathcal{Z}} \sigma_i^x \prod_{j=1}^{\mathcal{Z}} (1 - 4\sigma_{i+j}^z \sigma_{i-j}^z) + H_{edge}. \quad (\text{A1})$$

Here, H_{edge} represents the Hamiltonian representing all the connections at the edge. However, as stated in Ref. [59], describing the spin dynamics of the polarization wave using Hamiltonian in Eq. (A1) is not possible due to the interaction with next-nearest neighbors, which spoils the resonance condition. This issue can be addressed by assuming moderate values of the transverse magnetic field h^x that is greater than the next nearest-

neighbor interaction strength but less than the interaction strength of the nearest neighbors. These conditions, combined with a weak resonant transverse magnetic field, lead to a flipping sequence in the spin chain, giving rise to the polarization wave, thereby leading to a GHZ state, responsible for quantum advantage in sensing.

Appendix B: Gaussian and uniform disorder

Gaussian disorder. The strength of transverse magnetic field h^x involved in the Hamiltonian in Eq. (4) is chosen randomly from a Gaussian distribution. Hence the probability density function of choosing h^x from this distribution can be expressed as

$$P(h^x) = \frac{1}{\sigma_G \sqrt{2\pi}} \exp\left(-\frac{(h^x - \bar{h}_G^x)^2}{2\sigma_G^2}\right), \quad (\text{B1})$$

where \bar{h}_G^x is the mean value of the magnitude of the magnetic field along the transverse direction, and σ_G is the standard deviation of the distribution [68]. Here the subscript G in the mean and standard deviation represent the Gaussian distribution respectively. The quenched averaged value of the physical quantity, which is minimum uncertainty here, is given by $\langle \delta\omega \rangle = \int P(h^x) \delta\omega_{\min}(h^x) dh^x$.

Uniform disorder. In this case, h^x is distributed as

$$P(h^x) = \begin{cases} \frac{1}{b-a} & a \leq h^x \leq b, \\ 0 & \text{otherwise,} \end{cases} \quad (\text{B2})$$

where a and b are the lower and upper bounds of the range of the uniform distribution. The mean and standard deviation of the uniform distribution are given by $\bar{h}_U^x = \frac{a+b}{2}$ and $\sigma_U = \sqrt{\frac{(b-a)^2}{12}}$ respectively [69, 70]. In a similar fashion, quenched averaged quantity can be computed.